# Stable metal-organic frameworks modulated by doping $Tb^{3+}$ for multi-hazard detection and capture

Gao, Y.; Dai, Z.; Li, M.; Zhang, J.; Tanase, S.; Jiang, R.

**DOI**
10.1039/d2me00141a

**Publication date**
2023

**Document Version**
Final published version

**Published in**
Molecular Systems Design and Engineering

MSDE

PAPER

View Article Online
View Journal | View Issue





Cite this: *Mol. Syst. Des. Eng.*, 2023, **8**, 341

# Stable metal–organic frameworks modulated by doping $Tb^{3+}$ for multi-hazard detection and capture†

Yuan Gao,[a] Zhongran Dai,[b] Meng Li,[c] Jixiong Zhang,[c] Stefania Tanase *[d] and Rongli Jiang *[a]

Received 12th July 2022,
Accepted 1st November 2022

DOI: 10.1039/d2me00141a

rsc.li/molecular-engineering

Considering the discharge of radioactive and non-radioactive effluents during the mining process, we report on a study that proposes to use optical sensing for the detection and monitoring of pollutants. This is realized by doping of $Tb^{3+}$ ions in a metal–organic framework, namely UiO-66-$(COOH)_2$, and taking advantage of the host–guest interactions which allow analyte molecules to be pre-concentrated within the pores of the material, thus influencing the light absorption and emission profile of $Tb^{3+}$ ions. Concentration-dependent spectroscopy analysis shows that Tb@UiO-66-$(COOH)_2$ has a luminescence turn-off behaviour which is more sensitive in the presence of $Ni^{2+}$ and $UO_2^{2+}$ ions as compared with monovalent ($Ag^+$), bivalent ($Co^{2+}$), trivalent ($Fe^{3+}$), and tetravalent ($Sn^{4+}$) cations. The relative luminescent intensity ($I_0/I$) as a function of the concentrations of both $Ni^{2+}$ and $UO_2^{2+}$ shows a linear response in a broad concentration range ($10^{-7}$–$10^{-3}$ M). The limit of detection (LOD) for $Ni^{2+}$ is 5.7 μg $L^{-1}$, which is lower than the allowable concentration limit (0.02 mg $L^{-1}$) defined by the national environmental quality standard of surface water GB 3838. The LOD for $UO_2^{2+}$ is 0.02 μg $L^{-1}$, far below the World Health Organization maximum standards for potable water (30 μg $L^{-1}$). Therefore, Tb@UiO-66-$(COOH)_2$ enables the detection of these ions with high sensitivity. Notably, the optical response measured at low concentrations of $Ni^{2+}$ and $UO_2^{2+}$ is not affected even in the presence of interfering metallic ions. These results demonstrate for the first time that Tb@UiO-66-$(COOH)_2$ is a versatile multi-hazard sensor for the detection of non-radioactive and radioactive elements. It also opens opportunities for the selective adsorption and extraction of $UO_2^{2+}$ due to the high-stability functionality of Tb@UiO-66-$(COOH)_2$.

### Design, System, Application

The high coordination numbers and flexible coordination geometry of $Ln^{3+}$ ions pose great challenges in synthesizing the desired Ln-MOFs. We show here that the synthesis of these materials can be better controled by post-synthetic modification of a MOF and doping it with $Tb^{3+}$. The strategy was applied to obtain Tb@UiO-66-$(COOH)_2$. This material not only inherits the porosity and stability of pristine UiO-66-$(COOH)_2$, but also is endowed with distinct luminescent properties from $Tb^{3+}$. Taking these structural advantages, we demonstrate for the first time that Tb@UiO-66-$(COOH)_2$ is a versatile multi-hazard sensor for the detection of $Ni^{2+}$ and $UO_2^{2+}$ at low concentration even when coexisting with various interfering ions. We also show the promising opportunities for the selective adsorption and extraction of $UO_2^{2+}$ of Tb@UiO-66-$(COOH)_2$ due to its ultra-stability and high functionality. These studies bridge the gap between multi-hazard detection and improved accuracy in one platform. In comparison to other sensing materials, this area is still in its early stages of development. It is foreseen that the luminescent MOF sensor created using the post-synthetic method will open new avenues in the development of sensor devices.

## Introduction

The current energy crisis represents one major challenge in the world, and tremendous efforts are being made to relieve this issue. Before switching to a fully sustainable global energy landscape, coal still accounts for a significant share of the total electricity production, and coal-fired power plants currently fuel 37% of global electricity.[1] Figures from the International Energy Agency show that coal will still generate 25% of the world's electricity in 2040, retaining coal's position as the single largest source of electricity worldwide.[2]

[a] *School of Chemical Engineering and Technology, China University of Mining & Technology, Xuzhou, Jiangsu, 221116, China. E-mail: ronglij@cumt.edu.cn*
[b] *Key Discipline Laboratory for National Defense for Biotechnology in Uranium Mining and Hydrometallurgy, University of South China, Hengyang, Hunan, 421001, China*
[c] *State Key Laboratory of Coal Resources and Safe Mining, School of Mines, China University of Mining & Technology, Xuzhou, Jiangsu, 221116, China*
[d] *Van't Hoff Institute for Molecular Sciences, University of Amsterdam, Science Park 904, 1098 XH Amsterdam, The Netherlands. E-mail: s.grecea@uva.nl*

† Electronic supplementary information (ESI) available: Experimental details, PXRD, $N_2$ adsorption and photoluminescent spectra. See DOI: https://doi.org/10.1039/d2me00141a

However, the process of coal mining and related activities involves the discharge of a huge amount of effluent into the surface water, among which the non-radioactive $Ni^{2+}$ and radioactive $UO_2^{2+}$ are two representative hazardous species.[3] This makes mining activities the main source of contamination in the environment, posing serious problems to human health, and affecting ecological surroundings.[4,5]

Considering both non-radioactive and radioactive hazardous species, the development of advanced methods for accurate and sensitive detection of both $Ni^{2+}$ and $UO_2^{2+}$ is highly desirable in mineral prospecting and environmental contamination monitoring.[6] Multi-ion detection can be realized using instrumental or chemical methods. The instrumental methods, including ICP-MS, ESI-MS, and neutron activation analysis, enable to achieve low detection limits with high validity and repeatability. However, the expensive as well as complicated sample preparation, limit their applications.[7] The performance of chemical methods usually implies low cost, fast response, and no need for special instrumentation.[8] Nevertheless, their effectiveness is inhibited by the production of secondary pollutants, and the inability to operate under harsh conditions. Therefore, the development of advanced multi-ion detectors with easy handling, lower costs, and without hazardous wastes is great in demand.

Metal–organic frameworks (MOFs) form a special class of porous materials featuring excellent stability, high surface area, and tunable functionalities.[9] They have been extensively studied for applications in drug delivery and release,[10] gas storage and separation,[11] catalysis,[12] and chemical sensing.[13–18] Among different MOFs, lanthanide-based MOFs (Ln-MOFs) are relevant candidates for developing optical sensors due to their excellent optical properties through antenna effects and high color purity.[19–21] A number of Ln-MOFs have been designed and used to sense heavy metal ions,[22] toxic organic pollutants,[23,24] and volatile organic compounds (VOC).[21,25–27]

The unique photophysical properties of lanthanides, such as europium, terbium, and ytterbium, make their corresponding MOFs very attractive candidates for chemical sensing applications. In particular, their long-lived photoluminescence, narrow bandwidth emissions, and large Stokes shifts are highly sensitive upon the interaction with analytes. It has also been demonstrated that luminescence quenching is a more common phenomenon, which is generally caused by the structural collapse, cation exchange and the framework–guest interactions.[26,27] One great challenge to synthesize the desired Ln-MOFs arises from the high coordination numbers and flexible coordination geometry of $Ln^{3+}$ ions. Recent developments in MOFs synthesis methods, such as post-synthetic modification which is performed on the as-synthesised materials, provide an alternative approach to construct desired Ln-MOFs and exploit their unique properties.

Most MOFs have relatively low chemical stability under an acid/alkaline environment, hampering their structural modifications. Yet, there are a few MOFs with a very high surface area as well as high thermal stability.[28,29] Particularly, UiO-66 is well-known for its high stability and exceptional tunability and functionality arising from the metal oxide nodes being cub octahedral, namely $Zr_6O_4(OH)_4$, which enable 12-fold connections to adjacent 1,4-benzenedicarboxylate linkers. Due to the high oxidation number of $Zr^{4+}$, high charge density, and bond polarization, there are strong bonding interactions between $Zr^{4+}$ ions and oxygen atoms of the carboxylate ligands. Therefore, Zr-based MOFs have excellent resistance towards water, organic solvents, diluted acids as well as bases whilst accommodating guest molecules and maintaining the robust frameworks.[30] Recently, UiO-66 derivatives have been investigated for specific recognitions and sensing of $Cd^{2+}$, $Cu^{2+}$, and $UO_2^{2+}$ ions.[31–33] However, UiO-66 based multi-ion detection of both non-radioactive and radioactive species with improved accuracy, precision, selectivity, and reduced detection limit, is not yet explored.[6]

This study reports on a new approach to achieve the detection of multi-hazard quantitatively and qualitatively within one platform. The organic linker 1,2,4,5-benzenetetracarboxylic acid ($H_4$btec) and $Zr^{4+}$ were combined to obtain the pristine UiO-66-$(COOH)_2$, featuring abundant uncoordinated carboxylic functional groups. This material was then used for the post-synthesis of a $Tb^{3+}$-dopped MOF, namely Tb@UiO-66-$(COOH)_2$, which inherits the porosity and stability from UiO-66-$(COOH)_2$. The key advantage of Tb@UiO-66-$(COOH)_2$ is that the carboxylic functional groups of the organic linkers can be used as free sites to host various metal ion. In this work, using this strategy combined with the distinctive luminescent properties of $Tb^{3+}$ ions, we show that selective and sensitive recognition of $Ni^{2+}$ and $UO_2^{2+}$ is achieved in a wide concentration range, due to the high affinity of the framework towards $Ni^{2+}$ and $UO_2^{2+}$ on the basis of structural stability. Additionally, we demonstrate that Tb@UiO-66-$(COOH)_2$ performs exceptionally good in capturing uranium species in a broad pH range.

## Materials

All reactants were commercially available from Sigma-Aldrich, and the >99% purity grade allowed them to be used directly.

### Synthesis of UiO-66-$(COOH)_2$

The water stable UiO-66-$(COOH)_2$ was synthesized using modified earlier reported synthesis procedures.[34,35] In brief, 1,2,4,5-benzenetetracarboxylic acid ($H_4$btec) (0.63 g, 2.5 mmol) and zirconium tetrachloride ($ZrCl_4$) (0.61 g, 2.6 mmol) was dispersed in 20 mL distilled water under stirring. After well-mixing, the resulting solution was heated to ~100 °C and refluxed for 12 h, leading to a yellow solid. The isolated solid was washed with boiling water 3 times, and dried in the vacuum at 70 °C for 4 h, yielding a white powder.

 

### Synthesis of Tb@UiO-66-(COOH)$_2$

Tb@UiO-66-(COOH)$_2$ was synthesized by heating UiO-66-(COOH)$_2$ (0.25 g) and $Tb(NO_3)_3{\cdot}6H_2O$ (1.1 g, 2.5 mmol) in distilled water (25 mL) at 60 °C. The solid was isolated by centrifugation at 10 000 rpm, then thoroughly washed three times with distilled water to remove unreacted $Tb^{3+}$, and dried under vacuum at 70 °C.

### Physical methods

Infrared spectra (4000–400 cm$^{-1}$, resol. 0.5 cm$^{-1}$) were recorded on a Varian 660 Fourier-transform infrared (FTIR) spectrometer using KBr pellets and the transmission technique. Powder X-ray diffraction (PXRD) measurements were carried out on a Bruker AXS D8 Advance Diffractometer using Cu-Kα radiation ($\lambda$ = 0.154 nm, 35 kV, 40 mA). The data were collected from 5° to 60° with a turning speed of 2.0° min$^{-1}$. Thermogravimetric analysis (TGA) and differential scanning calorimetry (DSC) was performed using a NETZSCH Jupiter® STA 449F3 instrument. The measurements were done under air (20 mL min$^{-1}$) at 35–800 °C with a speed of 10 K min$^{-1}$. The elemental analysis and surface states of the materials were analyzed by X-ray photoelectron spectroscopy (XPS), which were carried out on a Thermo Fisher spectrometer (ESCALAB 250Xi, Thermo Fisher, USA) using a monochromatized Al Kα radiation ($h\nu$ = 1486.6 eV). Brunauer–Emmett–Teller (BET) specific surface area was calculated based on the N2 adsorption–desorption measured at 77 K on a ASAP 2020. The samples were activated at 300 °C overnight under vacuum. The scanning electron microscope (SEM) and energy-dispersive X-ray (EDX) analyses were performed on a Zeiss Sigma 300 scanning electron microscope. The concentration of $Tb^{3+}$ in aqueous was analyzed by an inductively coupled plasma optical emission spectrometer (ICP-OES).

## Results and discussion

### Materials characterization

To confirm the successful synthesis of Tb@UiO-66-(COOH)$_2$, a detailed structural analysis was conducted using FTIR, PXRD, TGA-DSC, and XPS. By comparing the FTIR spectra of UiO-66-(COOH)$_2$ and Tb@UiO-66-(COOH)$_2$ in Fig. 1(a), it is possible to identify the changes of the functional groups. Note that only two of the carboxylic groups of the organic ligands are coordinated to the $Zr^{4+}$ ions in pristine UiO-66. The IR characteristic band of the free carboxylic groups around 1700 cm$^{-1}$ ($\nu_{C=O}$ stretching vibration), becomes weaker after doping with lanthanide ions, thus confirming the coordination of $Tb^{3+}$ to benzenetetracarboxylic acid linkers.

Furthermore, the incorporation of $Tb^{3+}$ ions does not influence the crystallinity and thermal stability of the original framework, as confirmed by PXRD and TGA-DSC (Fig. 1(b) and (c)). The PXRD patterns of as-synthesized UiO-66-(COOH)$_2$ and Tb@UiO-66-(COOH)$_2$ are in good agreement with the simulated PXRD pattern of UiO-66.[36] As shown in

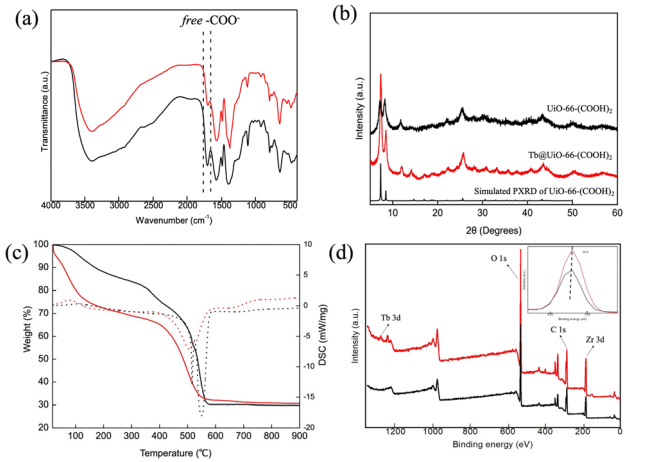


Fig. 1 FTIR spectra (a), PXRD patterns (b), TGA (continuous line) and DSC (dotted line) curves (c), and XPS analysis (d) of UiO-66-(COOH)$_2$ (black) and Tb@UiO-66-(COOH)$_2$ (red).

Fig. 1(b), Tb@UiO-66-(COOH)$_2$ contains the main crystallographic peaks at 7–8°, 12°, and 25°, indicating that MOF's purity and crystallinity were not influenced by the incorporation of $Tb^{3+}$ ions.[37] An important requirement for adsorbents is the material's stability. Thus, in the case of aqueous metal ions adsorption, a water-stable adsorbent is required, preferably with high resistance to acidic conditions. To assess the material's resistance under these conditions, Tb@UiO-66-(COOH)$_2$ was well dispersed in aqueous solutions with pH in the range 2 to 6 and adjusted with HCl and $Na_2CO_3$. Based on PXRD patterns (Fig. S1†), it can be concluded that the crystallinity is retained. Moreover, we have not detected aqueous-phase concentrations of $Tb^{3+}$ (ICP analysis), indicating a perfect resistance to acidic conditions. Fig. 2(c) shows that the thermal stability of the modified UiO-66 framework is preserved, as the appearance of rapid weight loss and the sharp exothermic peaks around 450 °C can be

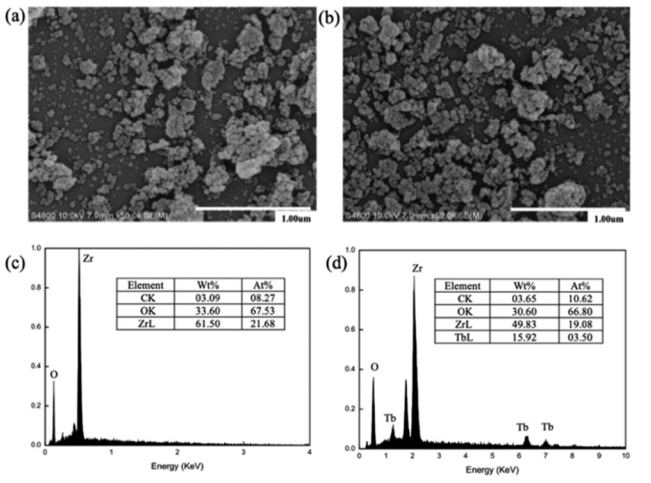


Fig. 2 SEM images of UiO-66-(COOH)$_2$ (a) and Tb@UiO-66-(COOH)$_2$ (b). The EDS analyses of UiO-66-(COOH)$_2$ (c) and Tb@UiO-66-(COOH)$_2$ (d).

considered as the collapse of the frameworks. For UiO-66-$(COOH)_2$, the residual amount after full combustion corresponds to *ca.* 29.8%. Due to the insertion of $Tb^{3+}$ ions in the frameworks, a higher residue of *ca.* 30.7% was observed for Tb@UiO-66-$(COOH)_2$.

Fig. 1(d) shows the characteristic Tb 3d peak at 1242 eV in Tb@UiO-66-$(COOH)_2$, which is not present in the spectrum of UiO-66-$(COOH)_2$.[31,38] The binding energies of O 1s shifted slightly from 531.98 eV to 531.87 eV, because the $Tb^{3+}$ coordination effect influences the bonding energy of O 1s.[39] Based on XPS, the weight percentage of terbium and zirconium are calculated to be 0.8% and 4.54% in Tb@UiO-66-$(COOH)_2$ respectively, and thus the ratio between incorporated terbium and zirconium atoms is calculated around 1 : 6.

The preserved structural integrity of Tb@UiO-66-$(COOH)_2$ and the successful $Tb^{3+}$-doping were also demonstrated using SEM and EDS. Fig. 2(a) and (b) show that the microstructure of Tb@UiO-66-$(COOH)_2$ is similar to that of UiO-66-$(COOH)_2$. Their similar morphology indicates that the structure is preserved upon introduction of $Tb^{3+}$. The particles constructed from a uniform distribution of crystallites are around 50 nm, which means they can be appropriately dispersed in aqueous media.[36] The EDS patterns (Fig. 2(c) and (d)) of UiO-66-$(COOH)_2$ and Tb@UiO-66-$(COOH)_2$ revealed the changes in the elemental composition upon doping with $Tb^{3+}$ ions. The atomic ratio of Zr (19.08%)/Tb (3.5%) was calculated to be approximately 6 : 1 in Tb@UiO-66-$(COOH)_2$, in consistence with the results from XPS analysis. Meanwhile, the Zr/O atomic ratio (3.5 : 66.8) was lower than that of Zr/O (19.08 : 66.8), since the carboxyl functional groups are partially coordinated to the metal ions. This indicates that free carboxylic acid groups still remain in the framework, therefore they can be used as active sites in recognizing and capturing metal ions.[40]

The porosity and surface area of the host framework are key features for the selective recognition of guest molecules. Therefore, we carried out $N_2$ adsorption–desorption isotherm experiments (Fig. S2†) of UiO-66-$(COOH)_2$ and Tb@UiO-66-$(COOH)_2$. The specific surface area of Tb@UiO-66-$(COOH)_2$ was calculated to be 157 $m^2\ g^{-1}$, lower than that of the pristine UiO-66-$(COOH)_2$ (190 $m^2\ g^{-1}$). The small reduction in BET surface area indicated the loading of $Tb^{3+}$ inside the original MOF. As compared with the literature values, the relatively smaller surface area of UiO-66-$(COOH)_2$ may arise from the pore's blocking with solvent molecules.[41]

The photoluminescent excitation and emission spectra of Tb@UiO-66-$(COOH)_2$ were measured for well-dispersed solutions. As shown in Fig. 3, the emission spectra of $Tb^{3+}$ excited at 300 nm revealed the well-resolved magnified luminescence of the f–f transition, attributed to the energy transfer from $btec^{4-}$ ligands to $Tb^{3+}$. The characteristic sharp bands at 490, 544, 585, and 620 nm are assigned to the $^5D_4 \rightarrow {}^7F_J$ ($J$ = 6, 5, 4, 3) transitions, indicating the potential to use this material as a luminescent probe in aqueous solutions.[42] Under UV light irradiation, Tb@UiO-66-$(COOH)_2$ shows green luminescence, which can also be observed visually (inset of Fig. 3).

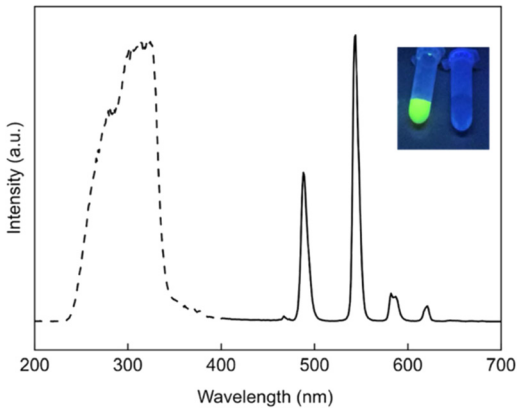


**Fig. 3** Photoluminescence spectra of Tb@UiO-66-$(COOH)_2$, measured in aqueous suspension. The inset shows a photograph of a sample illuminated using UV light ($\lambda_{ex}$ = 254 nm).

In the light of its inheriting structural features and luminescence properties, the chemical sensing properties of Tb@UiO-66-$(COOH)_2$ were first investigated by treating the material with a series of metal cations in water.[43] To investigate the potential of Tb@UiO-66-$(COOH)_2$ towards metal ions recognition, finely grounded powder of Tb@UiO-66-$(COOH)_2$ was immersed into $M^{z+}$ solutions of different valent ions ($M^{z+}$ = $Ag^+$, $Co^{2+}$, $Ni^{2+}$, $Fe^{3+}$, $Sn^{4+}$, and $UO_2{}^{2+}$),[44] in addition to a blank for comparison. The same spectral features were observed for the samples immersed in different solutions as those identified for the solid state materials. As shown in Fig. 4(a), the luminescence spectra of all samples displayed the characteristic transitions for $Tb^{3+}$ at 490, 544, 585, and 620 nm respectively, accompanying a quenching mechanism in which the antenna effect of $Tb^{3+}$ and organic ligands was perturbed by the introduced metal ions. The corresponding histograms of the emission intensity observed at 544 nm provided more intuitive information that $Ni^{2+}$ and $UO_2{}^{2+}$ led to a significant quenching effect whilst only a small effect was observed for other tested cations (Fig. 4(b)).

We studied luminescent behaviour under relatively low concentrations ($10^{-7}$–$10^{-3}$ M) to further investigate the sensitivity of Tb@UiO-66-$(COOH)_2$ as a luminescent probe for $Ni^{2+}$ and $UO_2{}^{2+}$. As shown in Fig. S3,† the luminescent

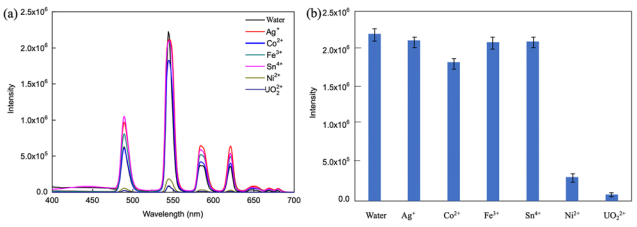


**Fig. 4** Luminescence intensity ($\lambda_{ex}$ = 300 nm) spectra of Tb@UiO-66-$(COOH)_2$ immersed in $10^{-9}$ M $M^{z+}$ solutions ($M^{z+}$ = $Ag^+$, $Co^{2+}$, $Ni^{2+}$, $Fe^{3+}$, $Sn^{4+}$ and $UO_2{}^{2+}$) (a) and the corresponding histograms of the luminescent intensity at 544 nm (b).

intensities of the $^5D_4 \rightarrow {}^7F_5$ transitions (544 nm) change by gradually increasing concentrations. A good linear relationship was observed only for the $Ni^{2+}$ and $UO_2^{2+}$ solutions, indicating a diffusion-controlled quenching process for these ions.[45] It is of particular interest that the time-dependent emission spectra demonstrate that Tb@UiO-66-$(COOH)_2$ towards $Ni^{2+}$ and $UO_2^{2+}$ are also very fast. As depicted in Fig. S4,† the emissions are significantly diminished and level off even within 1 min after the addition of $Ni^{2+}$ and $UO_2^{2+}$.

To quantitatively analyze the performance of Tb@UiO-66-$(COOH)_2$ as a luminescent probe for detecting $Ni^{2+}$ as well as $UO_2^{2+}$, we measured its quenching constants upon treatment with various cation solutions and using the Stern–Volmer equation:

$$I_0/I - 1 = K_{sv}[C]$$

Herein, $I_0$ and $I$ are the photoluminescent intensity of Tb@UiO-66-$(COOH)_2$ before and after the addition of metal ions. $[C]$ is different concentrations of $M^{z+}$. $K_{sv}$ represents the quenching effect coefficient of metal ions.[46,47]

As shown in Fig. 5(a), the quenching efficiency of $Ni^{2+}$ can be fitted to the following equation:

$$y = 0.2124 \times [C] + 1.4903$$

with the corresponding $K_{sv}$ calculated to be $2.124 \times 10^5$ $M^{-1}$. The $K_{sv}$ value is remarkably higher than usually measured for most MOFs-based cation sensing materials ($10^3$–$10^4$ $M^{-1}$), indicating a high selectivity towards $Ni^{2+}$. The detection limit (LOD) for $Ni^{2+}$ was estimated using the following equations:

$$LOD = 3\sigma/K_{sv}$$

where $\sigma$ is the standard deviation of replicate detections of blank solutions. Therefore, the detection limit is determined to be 5.7 μg $L^{-1}$, the value of which falls far below the tolerable maximum contamination concentration of 0.02 mg $L^{-1}$ $Ni^{2+}$ in drinking water as defined by China's water quality standards GB-3838.[48] In addition to fast response and high sensitivity performance, anti-interference ability is an important indicator to evaluate the feasibility of photoluminescent detection for practical application. Taking into account the ordinary turn-off luminescence in the presence of only $Ag^+$, $Co^{2+}$, $Fe^{3+}$, and $Sn^{4+}$, the selectivity and sensitivity towards $Ni^{2+}$ coexistence with these ions need to be confirmed. Therefore, in the presence of equilibrium interfering ion solutions composed of cations including $Ag^+$, $Co^{2+}$, $Fe^{3+}$ and $Sn^{4+}$, the competition experiments were conducted to explore the anti-interference ability of Tb@UiO-$(COOH)_2$. The emission spectra and corresponding photographs of luminescent intensities are shown in Fig. 5(b). Even in the presence of interfering analogue with different concentrations (10–$10^{-3}$ μM), the emission of $Tb^{3+}$ at 544 nm has almost no change, indicating the high affinity and interaction of the Tb@UiO-$(COOH)_2$ towards $Ni^{2+}$ ion.

The emission spectra of samples with various concentrations of $UO_2^{2+}$ ions were studied as well. From the slope of the fitting line derived from the Stern–Volmer plot (Fig. 6(a)), the following linear relation was derived:

$$y = 59.94 \times [C] + 2.7826$$

The value of $K_{sv}$ of $UO_2^{2+}$ ions was calculated to be $5.994 \times 10^7$ $M^{-1}$, which is larger as compared with previous reports (Table S1†). The detection limit of Tb@UiO-$(COOH)_2$ towards $UO_2^{2+}$ was calculated to be 0.02 μg $L^{-1}$ using the method discussed above. This is far below the maximum contamination standard (30 μg $L^{-1}$) in potable water based on the World Health Organization. Moreover, interfering experiments were carried out to evaluate the selectivity quenching ability of $UO_2^{2+}$. $Ag^+$, $Co^{2+}$, $Fe^{3+}$, and $Sn^{4+}$ are coexisting heavy metal with uranium in some mining activities,[49,50] thereby the photoluminescent changes were compared by monitoring emission peak at 544 nm before and after the addition of equilibrium interference ions composed of $Ag^+$, $Co^{2+}$, $Fe^{3+}$, and $Sn^{4+}$ into the $UO_2^{2+}$ solutions. As shown in Fig. 6(b), the intensities of $Tb^{3+}$ emission is unchanged, indicating that this Ln-MOF also has specific detection of $UO_2^{2+}$. To get further insight in the quenching phenomenon, the solid samples of Tb@UiO-66-

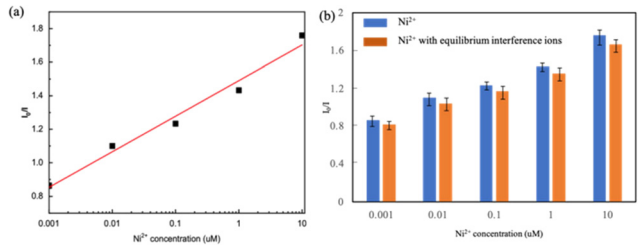


Fig. 5 Relationships between the concentration of $Ni^{2+}$ $I_0/I$. (a) The histograms of Tb@UiO-$(COOH)_2$ luminescent responses (monitored at 544 nm) with $Ni^{2+}$ at different concentrations. Blue bars represent the luminescent intensities when only $Ni^{2+}$ is present. Orange bars represent the change in the emission with the addition of equilibrium interference ions (b).

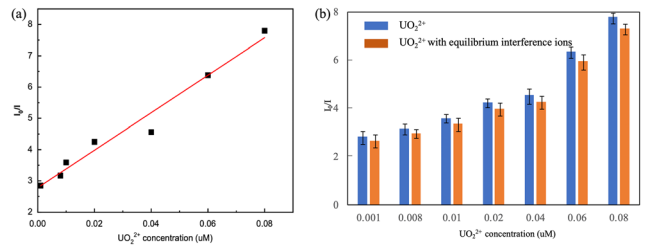


Fig. 6 Relationships between the concentration of $UO_2^{2+}$ and $I_0/I$. (a) The histograms of Tb@UiO-$(COOH)_2$ luminescent responses (monitored at 544 nm) with $UO_2^{2+}$ at different concentrations. Blue bars represent the luminescent intensities when only $UO_2^{2+}$ is present. Orange bars represent the change in the emission with the addition of equilibrium interference ions (b).

$(COOH)_2$ after being treated with $Ni^{2+}$ and $UO_2^{2+}$ solutions were also analysed. The PXRD patterns of the solid samples were analysed firstly (Fig. S5(a)†). The PXRD pattern is similar to the original material indicating that the structural integrity of the material is preserved. Moreover, ICP measurements have indicated that $Tb^{3+}$ are not present in the filtrate solutions. Altogether indicate that structural changes and cation exchange are not responsible for the luminescence quenching observed. At the same time, the FTIR spectra of the solids (see Fig. S5(b)†) showed the total disappearance of the free $-COO^-$ sites, indicating that the framework–cation interactions are responsible for the quenching mechanism. Two possible mechanisms may account for the high selectivity and sensitivity towards $Ni^{2+}$. A competition of absorption of excitation wavelength energy between the $Ni^{2+}$ aqueous solution and the carboxylate ligand may lead to a significant decrease of the transfer of excitation energy to $Tb^{3+}$ from the carboxylate ligand. It is also possible that there exists a small overlap between the absorption spectrum of the $Ni^{2+}$ aqueous solution and the strong emission band at 545 nm of Tb@UiO-$(COOH)_2$, therefore resulting in the quenching of luminescence.[51–53]

As the $K_{sv}$ ($UO_2^{2+}$) is two-order magnitude higher than $K_{sv}$ ($Ni^{2+}$), Tb@UiO-66-$(COOH)_2$ has higher sensitivity for the recognition of $UO_2^{2+}$ than $Ni^{2+}$. This high affinity towards $UO_2^{2+}$ inspired us to study the adsorption capacity of Tb@UiO-66-$(COOH)_2$. Detailed studies regarding the $UO_2^{2+}$ sorption ability were performed in the pH range from 2 to 6, in which the uranium species are mainly present in the form of $UO_2^{2+}$, while the Tb@UiO-66-$(COOH)_2$ structure remained crystalline and retained its structural integrity. By increasing the pH of the solution, Tb@UiO-66-$(COOH)_2$ shows an increased removal efficiency from *ca.* 5% to *ca.* 60%. The corresponding adsorption capacity increased from *ca.* 15 to 180 mg $g^{-1}$ (Fig. 7). Knowing that the uranium speciation is widely dependent on the pH, a less acidic solution can induce the protonation of the reactive sites.[54] As a result, the number of $COO^-$ negatively charged sites in Tb@UiO-66-$(COOH)_2$ increases as the pH of the solution increases.[55] Consequently, electrostatic attractions between the positive $UO_2^{2+}$ and negative adsorbents are stronger and the removal percentage increased. This behavior suggests that the sorption of the positively charged uranyl species by the carboxylic functional groups of the MOF is favorable.[56] The limitation of adsorption capacity does not limit its use in radioactive remediation, as this lanthanide MOF can be furtherly modified with abundant carboxyl groups that will help to improve the adsorption performance.

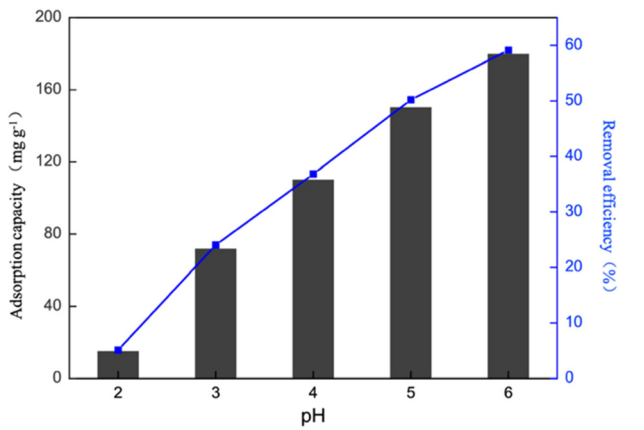


Fig. 7 Adsorption capacity (blue line) and removal efficiency (black histograms) of $UO_2^{2+}$ by Tb@UiO-66-$(COOH)_2$ at pH ranging from 2 to 6.

## Conclusions

We have synthesized a stable luminescent Tb@UiO-66-$(COOH)_2$ sensing probe by using a post-synthetic functionalized method and characterized it in detail by spectroscopic, surface characterization, and analytic techniques. Given the remarkable stability of the as-synthesized Tb@UiO-66-$(COOH)_2$, the evaluation of its chemical sensing properties in different chemical environments is possible. Our study demonstrates that Tb@UiO-66-$(COOH)_2$ material is a versatile multi-hazard sensor that can be used for the identification and quantification of both radioactive and nonradioactive species. Specifically, it retains a highly selective luminescent response to $Ni^{2+}$ and $UO_2^{2+}$ even when coexisting with various interfering ions. The high quenching effect observed clearly indicates a high sensitivity towards the radioactive and nonradioactive hazards. The negative carboxylate functional groups in the Tb@UiO-66-$(COOH)_2$ framework play a key role in the adsorption of positive $UO_2^{2+}$ by predominant electrostatic interactions. Therefore, Tb@UiO-66-$(COOH)_2$ shows high sensitivity for $UO_2^{2+}$ detection as well as selective adsorption, with a maximum adsorption capacity of 180 mg $g^{-1}$ at pH = 6. This work demonstrates for the first time that Tb@UiO-66-$(COOH)_2$ has a strong potential for applications aimed at monitoring multi-hazards of $Ni^{2+}$ and $UO_2^{2+}$ species sensitively as well as applications related to the recycling of nuclear fuel wastes in aqueous solutions.

## Author contributions

Yuan Gao: designed experiments, analysed the data, and contributed to the writing of the manuscript. Zhongran Dai: collected the $UO_2^{2+}$ adsorption data. Meng Li: performed the analysis of experimental data. Jixiong Zhang: provided instrumentation and analysis tools. Stefania Tanase: performed data analysis, provided conceptual input and contributed to the writing of the manuscript. Rongli Jiang: conducted a research and investigation process.

## Conflicts of interest

There are no conflicts to declare.

## Acknowledgements

This work is supported by the National Science Fund for Distinguished Young Scholars (No. 51725403), the National Natural Science Foundation of China (No. 52004271), and Hunan Provincial Natural Science Foundation for Excellent Young Scholars (No. 2020JJ3028). The "Qihang Plan" fund of the China University of Mining and Technology is acknowledged. This work is also part of the Research Priority Area Sustainable Chemistry of the University of Amsterdam, **https://suschem.uva.nl**.

## Notes and references

1 A. Zhou, J. Hu and K. Wang, *Environ. Earth Sci.*, 2020, **79**, 1–15.
2 T. Ahmad and D. Zhang, *Energy Rep.*, 2020, **6**, 1973–1991.
3 V. K. Mishra, A. R. Upadhyaya, S. K. Pandey and B. Tripathi, *Bioresour. Technol.*, 2008, **99**, 930–936.
4 A. Kong, Y. Ji, H. Ma, Y. Song, B. He and J. Li, *J. Cleaner Prod.*, 2018, **192**, 801–808.
5 Y. Chen, X. Jiang, Y. Wang and D. Zhuang, *Process Saf. Environ. Prot.*, 2018, **113**, 204–219.
6 W. Liu, Y. Wang, L. Song, M. A. Silver, J. Xie, L. Zhang, L. Chen, J. Diwu, Z. Chai and S. Wang, *Talanta*, 2019, **196**, 515–522.
7 D. Rathore, *Talanta*, 2008, **77**, 9–20.
8 J. K. Fink, *The Chemistry of Environmental Engineering*, John Wiley & Sons, 2020.
9 H.-C. Zhou, J. R. Long and O. M. Yaghi, *Chem. Rev.*, 2012, **112**, 673–674.
10 P. Horcajada, C. Serre, M. Vallet-Regí, M. Sebban, F. Taulelle and G. Férey, *Am. Ethnol.*, 2006, **118**, 6120–6124.
11 H. Li, K. Wang, Y. Sun, C. T. Lollar, J. Li and H.-C. Zhou, *Mater. Today*, 2018, **21**, 108–121.
12 D. Farrusseng, S. Aguado and C. Pinel, *Angew. Chem., Int. Ed.*, 2009, **48**, 7502–7513.
13 Y. Cui, B. Li, H. He, W. Zhou, B. Chen and G. Qian, *Acc. Chem. Res.*, 2016, **49**, 483–493.
14 L. E. Kreno, K. Leong, O. K. Farha, M. Allendorf, R. P. Van Duyne and J. T. Hupp, *Chem. Rev.*, 2012, **112**, 1105–1125.
15 J. F. Olorunyomi, S. T. Geh, R. A. Caruso and C. M. Doherty, *Mater. Horiz.*, 2021, **8**, 2387–2419.
16 I. Stassen, N. Burtch, A. Talin, P. Falcaro, M. Allendorf and R. Ameloot, *Chem. Soc. Rev.*, 2017, **46**, 3185–3241.
17 L. Li, Q. Chen, Z. Niu, X. Zhou, T. Yang and W. Huang, *J. Mater. Chem. C*, 2016, **4**, 1900–1905.
18 H. Sohrabi, P. S. Sani, Y. Orooji, M. R. Majidi, Y. Yoon and A. Khataee, *Food Chem. Toxicol.*, 2022, 113176.
19 S.-N. Zhao, G. Wang, D. Poelman and P. V. D. Voort, *Materials*, 2018, **11**, 572.
20 W. Liu, C. Chen, Z. Wu, Y. Pan, C. Ye, Z. Mu, X. Luo, W. Chen and W. Liu, *ACS Sustainable Chem. Eng.*, 2020, **8**, 13497–13506.
21 S. Wang, B. Sun, Z.-M. Su, G. Hong, X. Li, Y. Liu, Q.-Q. Pan and J. Sun, *Inorg. Chem. Front.*, 2022, **9**, 3259–3266.
22 P. Samanta, A. V. Desai, S. Sharma, P. Chandra and S. K. Ghosh, *Inorg. Chem.*, 2018, **57**, 2360–2364.
23 L. Rani, J. Kaushal, A. L. Srivastav and P. Mahajan, *Environ. Sci. Pollut. Res.*, 2020, **27**, 44771–44796.
24 M. Wagner, K.-Y. A. Lin, W.-D. Oh and G. Lisak, *J. Hazard. Mater.*, 2021, **413**, 125325.
25 H. Yu, Q. Liu, J. Li, Z.-M. Su, X. Li, X. Wang, J. Sun, C. Zhou and X. Hu, *J. Mater. Chem. C*, 2021, **9**, 562–568.
26 S. Khatua, C. Krishnaraj, D. C. Baruah, P. Van Der Voort and H. S. Jena, *Dalton Trans.*, 2021, **50**, 14513–14531.
27 S. Yu, J. X. Li, G. Zeng, Y. H. Xing, F. Y. Bai and Z. Shi, *Inorg. Chem.*, 2022, **61**, 3111–3120.
28 S. Zuluaga, E. M. Fuentes-Fernandez, K. Tan, F. Xu, J. Li, Y. J. Chabal and T. Thonhauser, *J. Mater. Chem. A*, 2016, **4**, 5176–5183.
29 Z. Hu, B. J. Deibert and J. Li, *Chem. Soc. Rev.*, 2014, **43**, 5815–5840.
30 H. Zhang, P. Xiong, G. Li, C. Liao and G. Jiang, *TrAC, Trends Anal. Chem.*, 2020, 116015.
31 X.-X. Peng, G.-M. Bao, Y.-F. Zhong, J.-X. He, L. Zeng and H.-Q. Yuan, *Spectrochim. Acta, Part A*, 2020, **240**, 118621.
32 W. Yang, Q. Pan, S. Song and H. Zhang, *Inorg. Chem. Front.*, 2019, **6**, 1924–1937.
33 X. Qin, W. Yang, Y. Yang, D. Gu, D. Guo and Q. Pan, *Inorg. Chem.*, 2020, **59**, 9857–9865.
34 Q. Yang, S. Vaesen, F. Ragon, A. D. Wiersum, D. Wu, A. Lago, T. Devic, C. Martineau, F. Taulelle and P. L. Llewellyn, *Angew. Chem., Int. Ed.*, 2013, **52**, 10316–10320.
35 Y. Gao, Y. Pan, Z. Zhou, Q. Tian and R. Jiang, *Molecules*, 2022, **27**, 1208.
36 Y. Han, M. Liu, K. Li, Y. Zuo, Y. Wei, S. Xu, G. Zhang, C. Song, Z. Zhang and X. Guo, *CrystEngComm*, 2015, **17**, 6434–6440.
37 D. Zou and D. Liu, *Mater. Today Chem.*, 2019, **12**, 139–165.
38 X. Zhang, W. Zhang, G. Li, Q. Liu, Y. Xu and X. Liu, *Microchim. Acta*, 2020, **187**, 122.
39 Z. Xiaoxiong, Z. Wenjun, L. Cuiliu, Q. Xiaohong and Z. Chengyu, *Inorg. Chem.*, 2019, **58**, 3910–3915.
40 Q. Yu, Z. Li, Q. Cao, S. Qu and Q. Jia, *TrAC, Trends Anal. Chem.*, 2020, 115939.
41 X.-X. Peng, G.-M. Bao, Y.-F. Zhong, L. Zhang, K.-B. Zeng, J.-X. He, W. Xiao, Y.-F. Xia, Q. Fan and H.-Q. Yuan, *Food Chem.*, 2020, **343**, 128504.
42 A. Silversmith, D. Boye, K. Brewer, C. Gillespie, Y. Lu and D. Campbell, *J. Lumin.*, 2006, **121**, 14–20.
43 M. Eddaoudi, H. Li and O. Yaghi, *J. Am. Chem. Soc.*, 2000, **122**, 1391–1397.
44 X. Liu, Z. Bai, H. Shi, W. Zhou and X. Liu, *Nat. Hazards*, 2019, **99**, 1163–1177.
45 G. Ji, J. Liu, X. Gao, W. Sun, J. Wang, S. Zhao and Z. Liu, *J. Mater. Chem. A*, 2017, **5**, 10200–10205.
46 H. Boaz and G. Rollefson, *J. Am. Chem. Soc.*, 1950, **72**, 3435–3443.
47 L. Liu, C. Zhang, Y. Yu and F. Chen, *Microchim. Acta*, 2018, **185**, 514.

48 Q.-H. Zhang, Y.-Z. Wei, J.-H. Cao and S. Yu, *Huanjing Kexue*, 2018, **39**, 1598–1607.
49 B. J. Alloway, *Heavy metals in soils: trace metals and metalloids in soils and their bioavailability*, Springer Science & Business Media, 2012.
50 S. Mortazavi, G. Mortazavi and M. Paknahad, *Environ. Sci. Pollut. Res.*, 2016, **23**, 22220.
51 H. Xu, F. Liu, Y. Cui, B. Chen and G. Qian, *Chem. Commun.*, 2011, **47**, 3153–3155.
52 W. Sun, J. Wang, H. Liu, S. Chang, X. Qin and Z. Liu, *Mater. Lett.*, 2014, **126**, 189–192.
53 S. S. Nagarkar, B. Joarder, A. K. Chaudhari, S. Mukherjee and S. K. Ghosh, *Am. Ethnol.*, 2013, **125**, 2953–2957.
54 C. Chisholm-Brause, S. D. Conradson, C. Buscher, P. G. Eller and D. E. Morris, *Geochim. Cosmochim. Acta*, 1994, **58**, 3625–3631.
55 F. Yang, S. Xie, G. Wang, C. W. Yu, H. Liu and Y. Liu, *Environ. Sci. Pollut. Res.*, 2020, 1–13.
56 N. Panagiotou, I. Liatsou, A. Pournara, G. K. Angeli, R. M. Giappa, E. Tylianakis, M. J. Manos, G. E. Froudakis, P. N. Trikalitis and I. Pashalidis, *J. Mater. Chem. A*, 2020, **8**, 1849–1857.

 